Supplementary Information (SI) for ChemComm.

Supporting Information

Enhancing Interfacial Electrocatalysts by Engineering Monomer Composition and Sequence of Metallo-oligomer Monolayers

Jing Li,[1,2] Chang Wei,[1,2] Lingyun Shen,[1,2] Yongfang Li,[1,2] Xuan Pang,[1,2] Mao Li[1,3*]

[1]*State Key Laboratory of Polymer Physics and Chemistry, Changchun Institute of Applied Chemistry, Chinese Academy of Sciences, Changchun 130022, China.*
[2]*School of Applied Chemistry and Engineering, University of Science and Technology of China, Hefei 230026, China.*
[3]*State Key Laboratory of Supramolecular Structure and Materials, College of Chemistry, Jilin University, Changchun, 130012, China. E-mail:* Limao@jlu.edu.cn

Table of Contents

1. Supplemental Figures and Notes **1**

UV-vis absorbance of SAMs and iterative monomer in solution 1

UV-vis absorbance and CVs of SAMs on ITO 1

CVs of iterative monomer 2

CVs of homo-oligomer monolayers 2

AFM characterization of homo-oligomer monolayers 3-5

CVs and UV-vis absorbance of hetero-oligomer monolayers 5-6

AFM characterization of hetero-oligomer monolayers 7

Electrocatalytic water oxidation 8-9

Characterizations of organic synthesis 10-21

2. Supplemental Synthesis **21**

3. Supplemental Methods **24**

4. Supplemental References **25**

1. Supplemental Figures and Notes

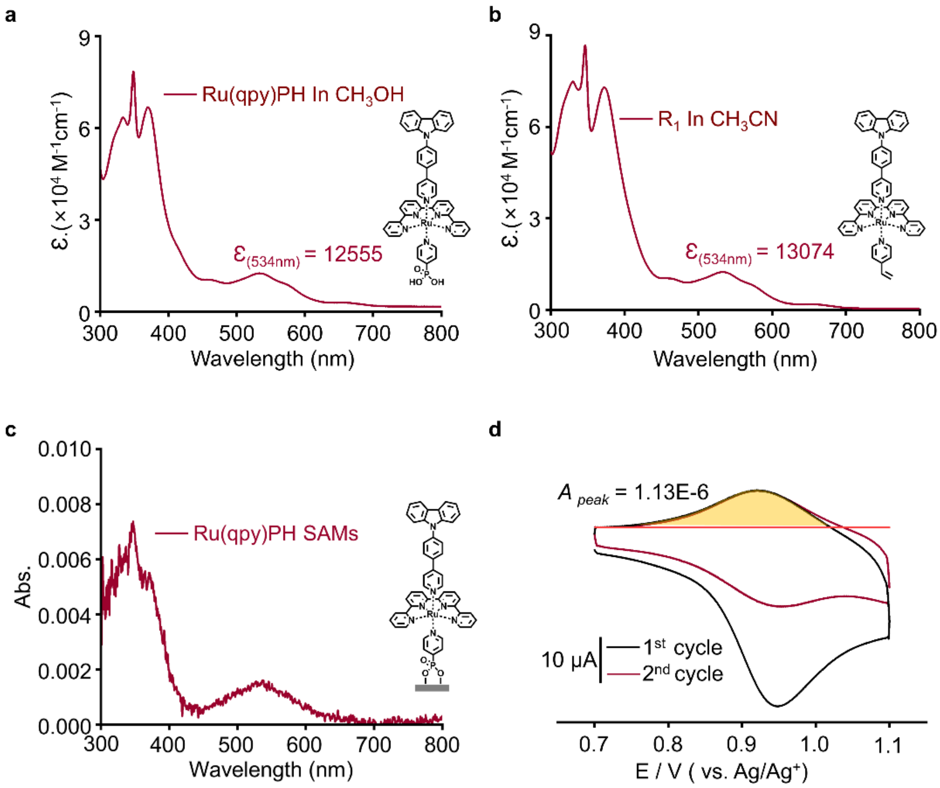

Figure S1. Calculation of the density of surface coverage. (a) UV-vis absorption spectrum of Ru(qpy)PH in CH_3OH. (b) UV-vis absorption spectrum of R_1 in CH_3CN. (c) UV-vis absorption spectrum of self-assembled monolayer (SAM) on indium tin oxide (ITO) fabricated by self-assembly of Ru(qpy)PH. (d) Cyclic voltammetry (CV) of SAM/ITO at the anodic scan of 100 mV/s in the monomer-free electrolyte. The density of surface coverage of 0.75 units/nm^2 is obtained from (a) and (c), according to the format: $\Gamma = A(\lambda_{peak})/\varepsilon(\lambda_{peak})/1000$. According to the redox area in (d), the density of surface coverage is calculated to be 0.71 units/nm^2, which is similar to the value obtained by the absorption spectrum as the former.

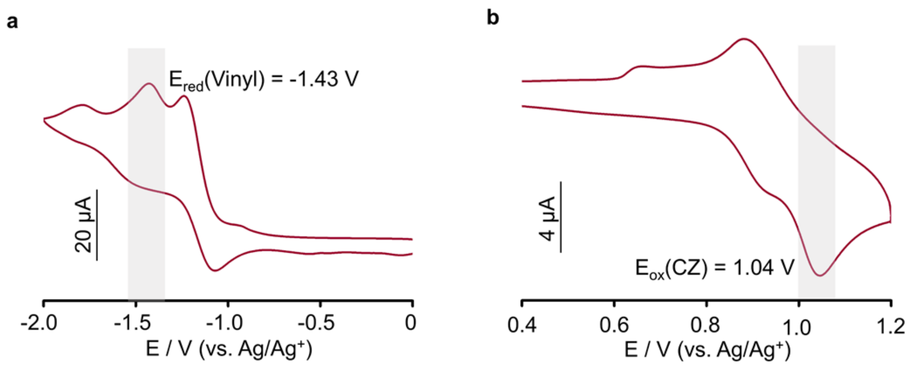

Figure S2. Electrochemical characterization of monomer R_1. (a,b) First cyclic CVs of 0.5 mM R_1 in 0.1 M TBAP (tetra-n-butylammonium perchlorate) CH_3CN solution at a scan rate of 100 mV/s on glassy carbon. In (a), the reductive peak of vinyl is −1.43 V vs Ag/Ag^+. In (b), the oxidative peak of carbazole is located at 1.04 V vs Ag/Ag^+, and a tiny reductive peak of 3,3′-bicarbazolyls is found at 0.60–0.70 V.

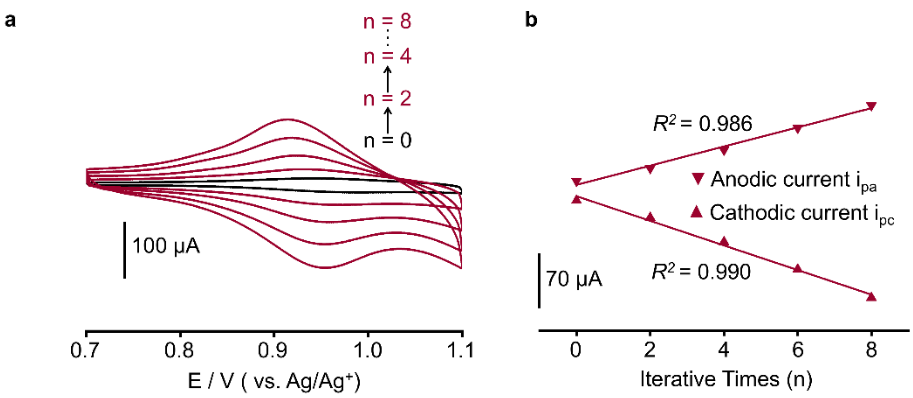

Figure S3. CV monitoring of homo-oligomer monolayers. (a) Height-dependent CVs of homo-oligomer monolayers in 0.1 M TBAP CH_3CN at a scan rate of 100 mV/s. (b) The linear relationships of redox peak current with iterative times.

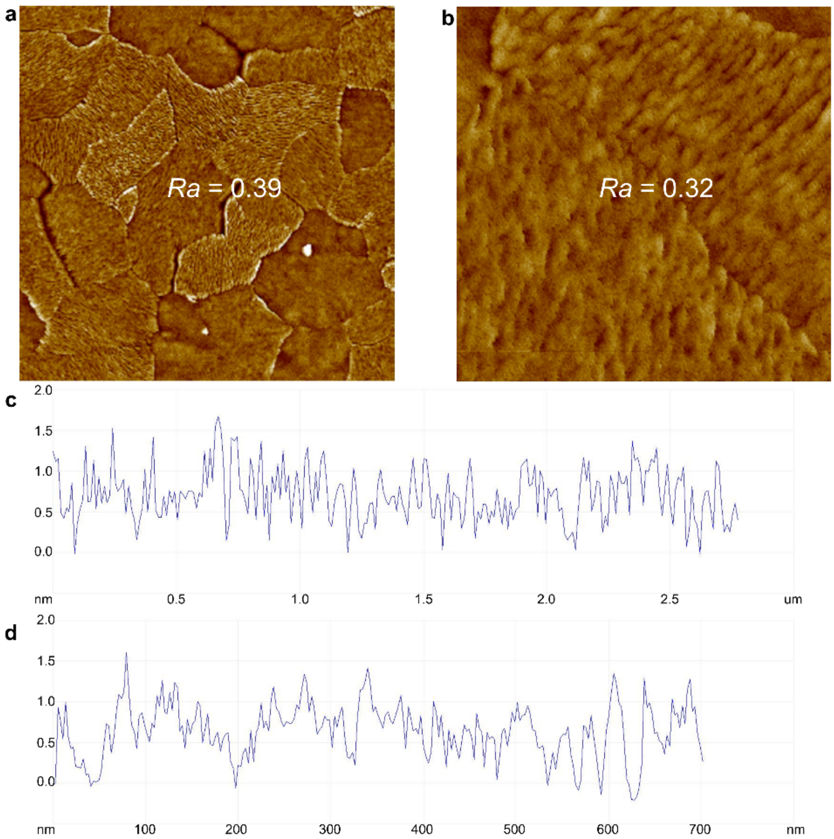

Figure S4. Atomic force microscope (AFM) characterization of ITO/Si. AFM images with different sizes of 2.0 × 2.0 μm^2 (a) and 0.50 × 0.50 μm^2 (b), and corresponding height changes (c,d) in diagonal lines of (a) and (b), respectively.

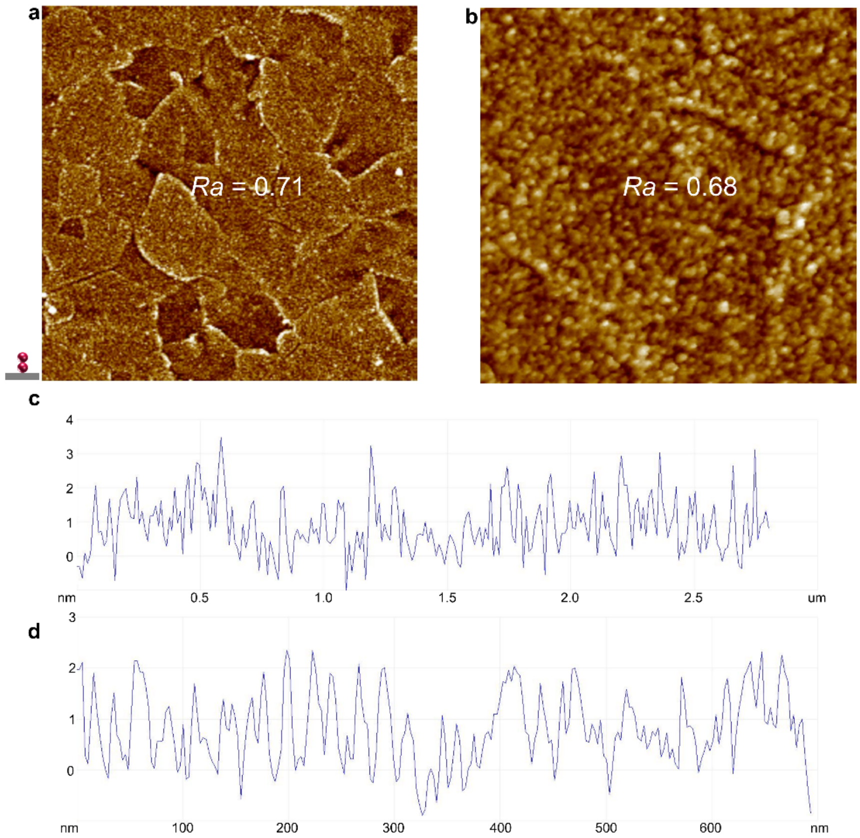

Figure S5. AFM characterization of homo-2mer monolayers/ITO/Si. AFM images with different sizes of 2.0 × 2.0 μm^2 (a) and 0.50 × 0.50 μm^2 (b), and corresponding height changes (c,d) in diagonal lines of (a) and (b), respectively.

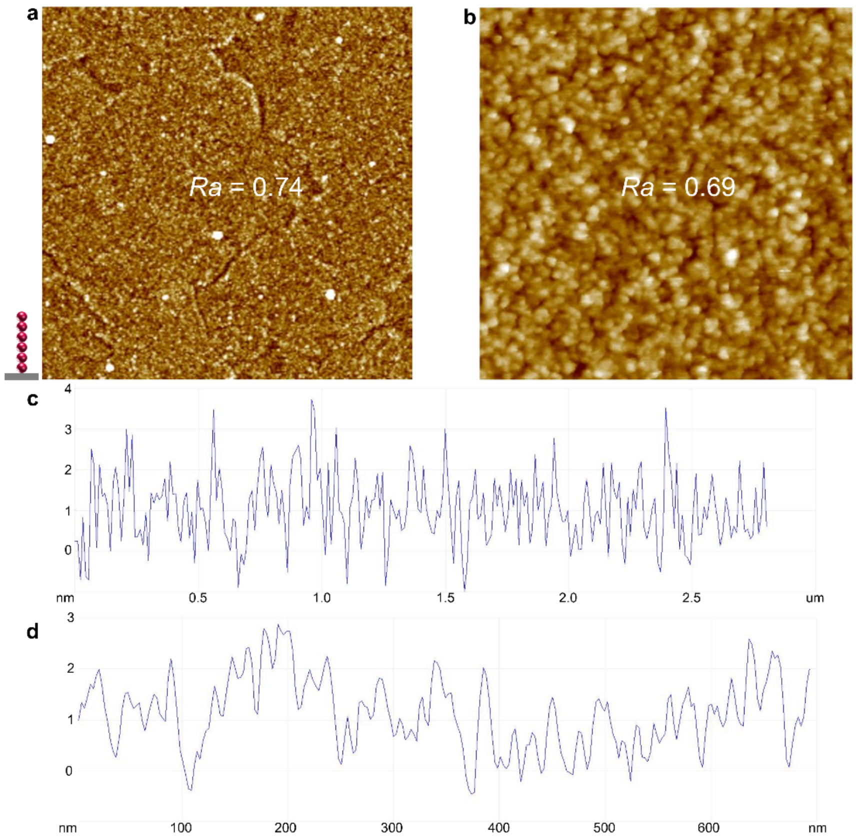

Figure S6. AFM characterization of homo-6mer monolayers/ITO/Si. AFM images with different sizes of 2.0 × 2.0 μm^2 (a) and 0.50 × 0.50 μm^2 (b), and corresponding height changes (c,d) in diagonal lines of (a) and (b), respectively.

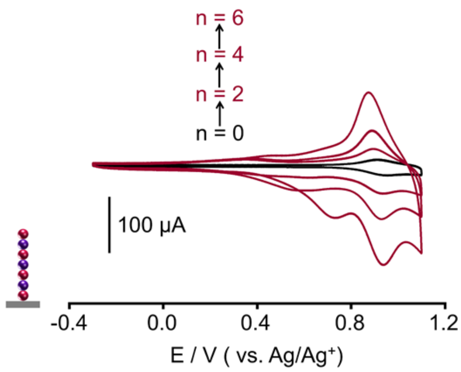

Figure S7. Height-dependent CVs of hetero-oligomer monolayers in 0.1 M TBAP CH_3CN at a scan rate of 100 mV/s. The redox peak of $Ru^{2+/3+}$ of R_2 ($E_{1/2}$ around 0.37 V vs Ag/Ag$^+$) exhibits progressively irreversible, possibly due to the extensive voltage scanning. In contrast, the redox peak current of $Ru^{2+/3+}$ of R_1 at 0.90 V vs Ag/Ag$^+$ still shows a regular increase with the increase of molecular lengths, demonstrating the controlled electrochemical reactions.

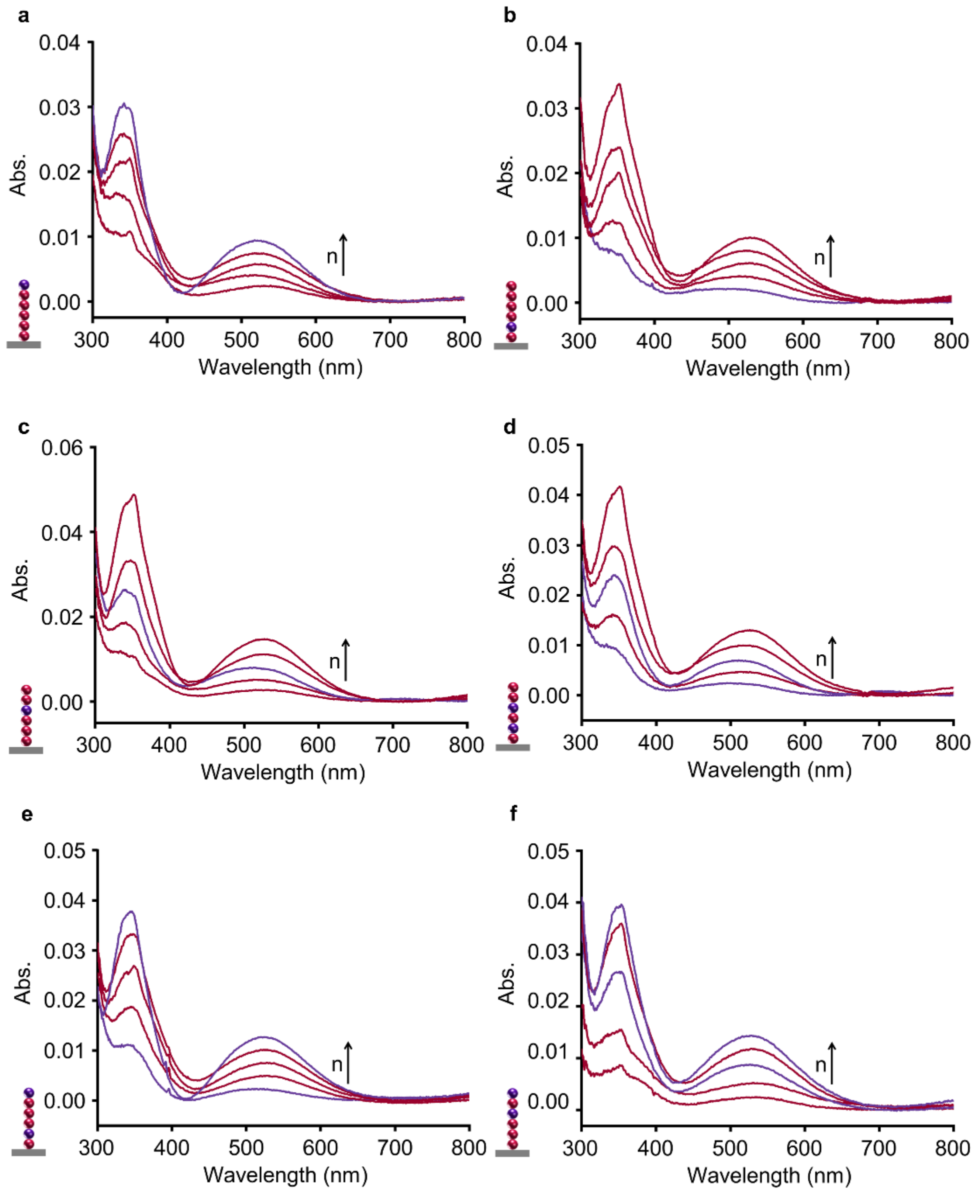

Figure S8. Height-dependent UV-vis absorption spectra of hetero-oligomer monolayers of difference sequences.

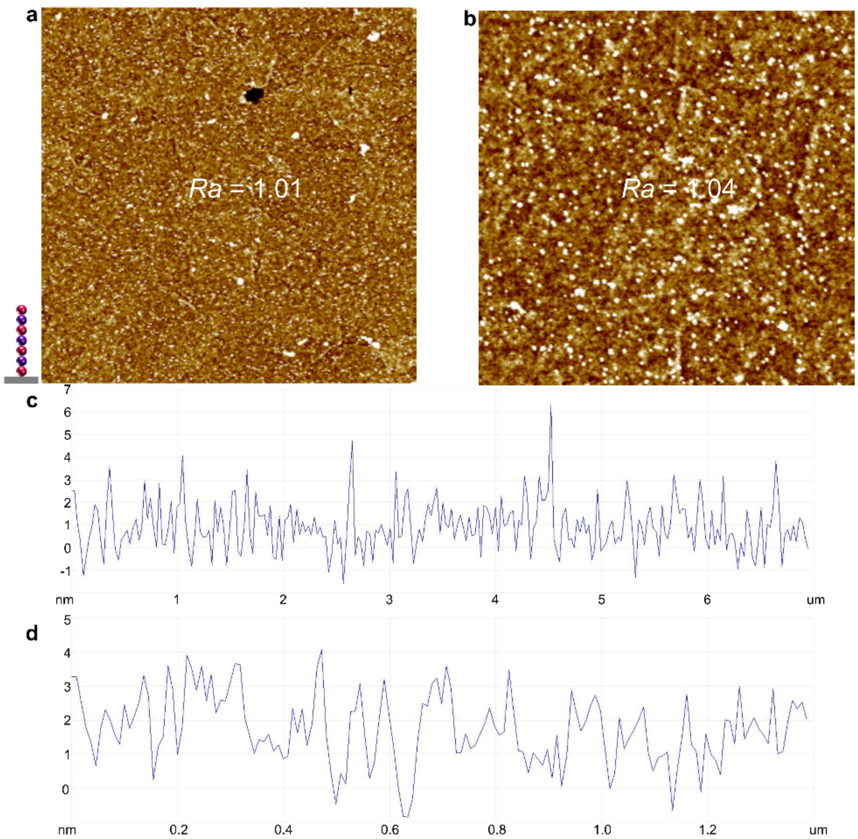

Figure S9. AFM characterization of hetero-7mer monolayers /ITO/Si. AFM images with different sizes of 5.0 × 5.0 μm² (a) and 2 × 2 μm² (b), and corresponding height changes (c,d) in diagonal lines of (a) and (b), respectively. The black dot in (a) represents the defects in the ITO.

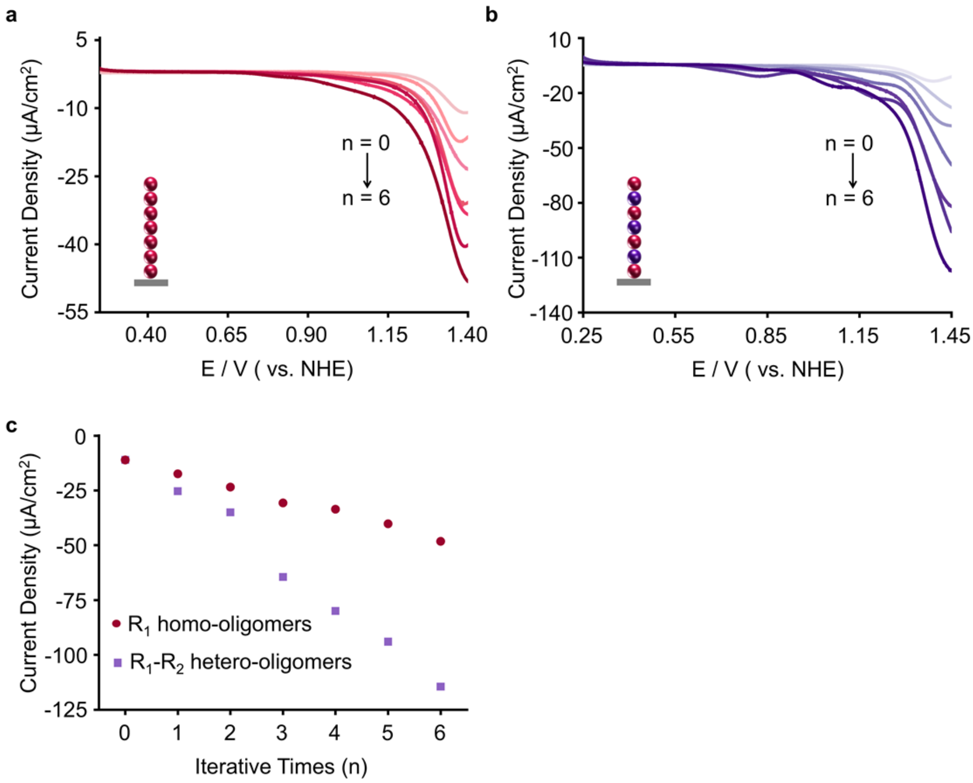

Figure S10. Length-dependent electrocatalytic. (a,b) Linear sweep voltammetry (LSV) curves for homo-oligomer (a) and hetero-oligomer (b) with different molecular lengths in pH = 1.0, 0.1 M $HClO_4$ aqueous solution at a scan rate of 20 mV/s. (c) Catalytic current densities of homo-oligomer and hetero-oligomer at 1.4 V vs. NHE as a function of iterative times. The catalytic current density of hetero-oligomer increases by nearly 100% compared with the homo-monolayer with the same length.

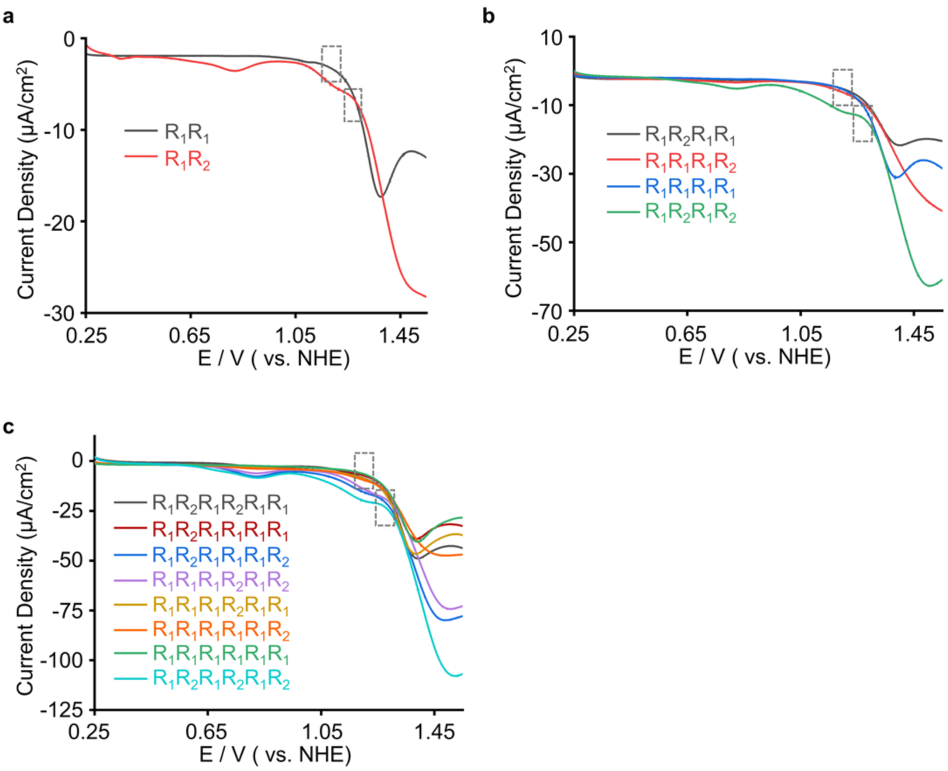

Figure S11. Sequence-controlled electrocatalytic. LSV curves of 2mer (a), 4mer (b), and 6mer (c) monolayers with different sequences. For monolayers with the same length, the onset potential (frame) is depressed when R_1 is the end-capping of monolayers compared to that when R_2 is located at the terminal.

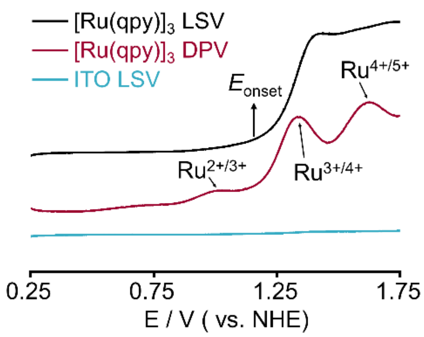

Figure S12. LSV curves for $[Ru(qpy)]_3$ (black) and blank ITO (blue) in pH = 1.0, 0.1 M $HClO_4$ aq (scan rate, 20 mV/s); Differential Pulse Voltammetry (DPV) curve for $[Ru(qpy)]_3$ (red) in pH = 1.0, 0.1 M $HClO_4$ aq (step potential = 4 mV, amplitude = 50 mV, frequency = 10 s^{-1}, modulation time = 0.05 s).

Analysis of the electrocatalytic water oxidation process as an example of homo-3mer monolayers. Under electrochemical conditions, the monolayers initially exhibit $Ru^{2+/3+}$ peak following oxidation, yielding $Ru^{3+/4+}$ peak under further oxidation.[1] The subsequent oxidation step is accompanied by the nucleophile attack of water molecule on the metal centers, leading to the formation of the seven-coordinated $Ru^{V} = O$; further water molecule attack facilitate oxygen release through electron transfer and proton coupling.[2-5] The blank ITO does not work in the catalysis.

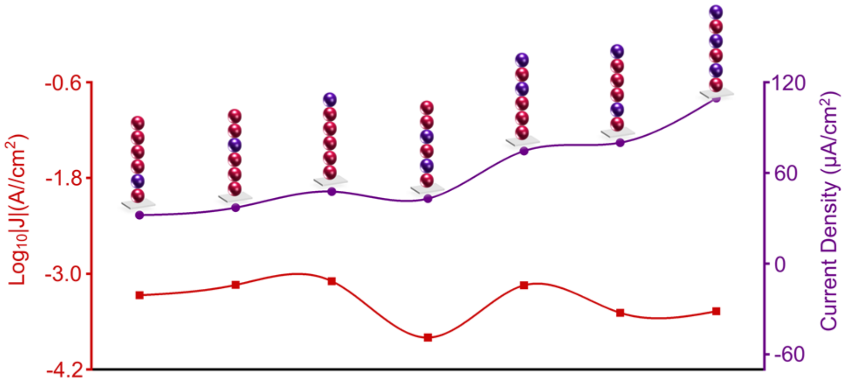

Figure S13. Conductance at 0.5 V and catalytic current density of hetero-6mer monolayers.

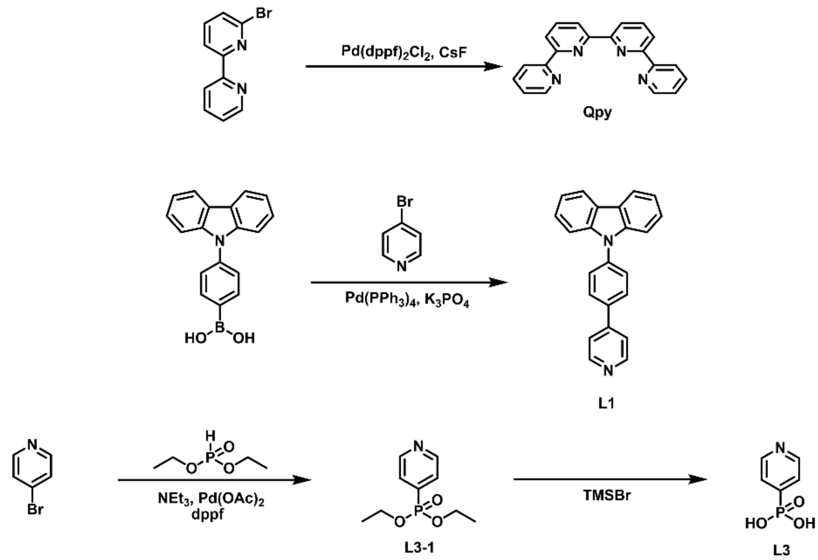

Figure S14. Synthesis routes of the ligands of monomer R_1 and SAMs.

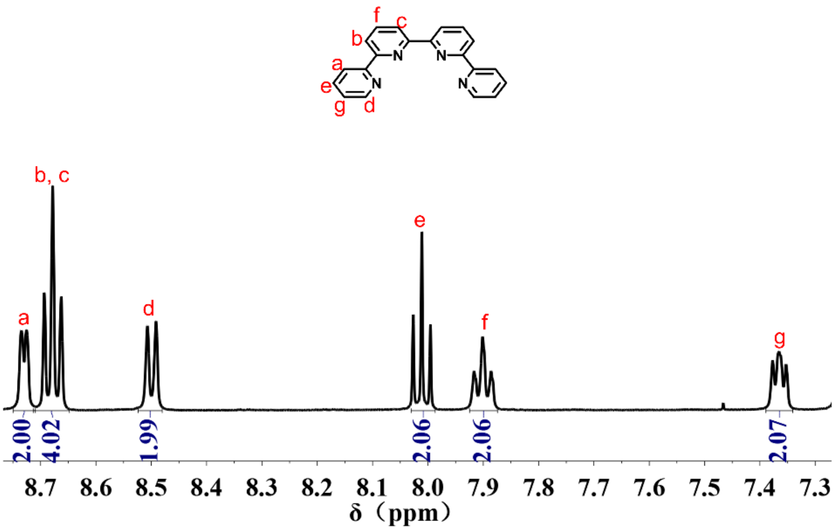

Figure S15. ^{1}H nuclear magnetic resonance (NMR) spectrum of 2,2':6',2'':6'',2'''-quaterpyridine (**qpy**) in $CDCl_3$.

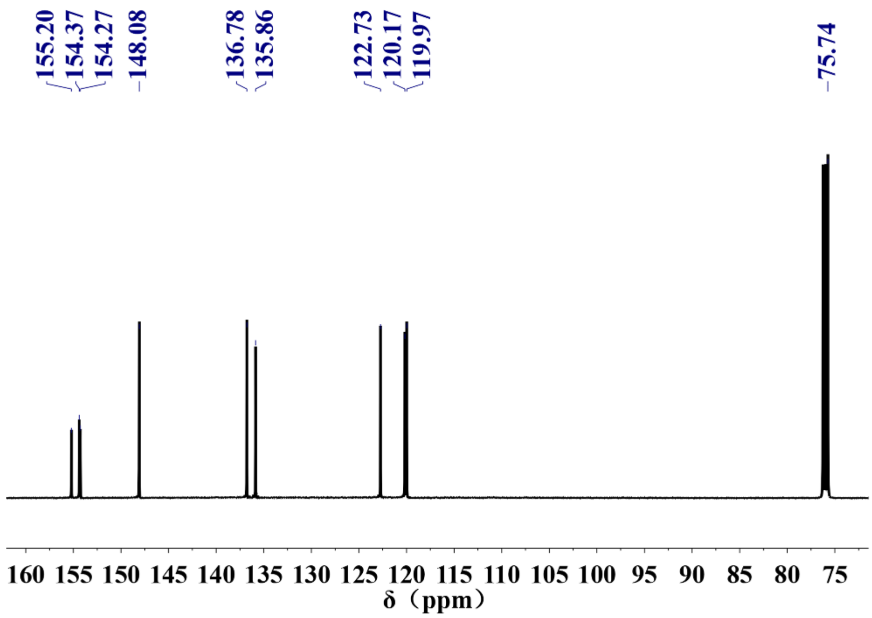

Figure S16. ^{13}C NMR spectrum of **qpy** in $CDCl_3$.

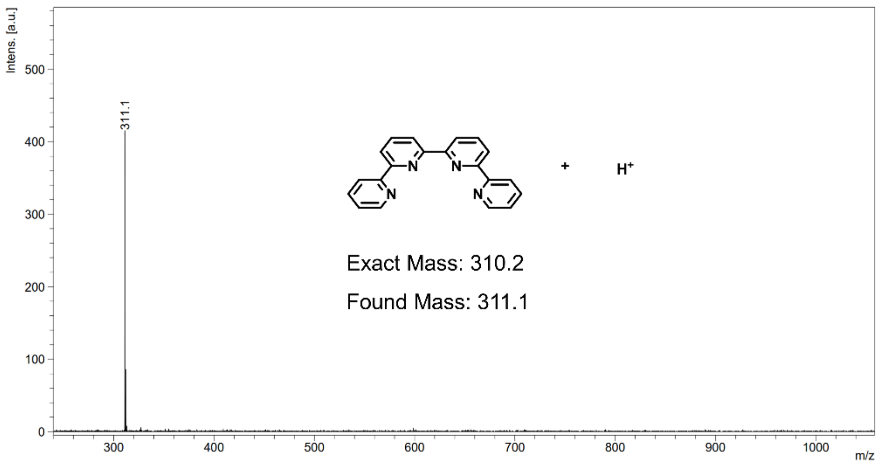

Figure S17. Matrix-assisted laser desorption ionization-time of flight (MALDI-TOF) mass spectrum of **qpy** in CH_2Cl_2.

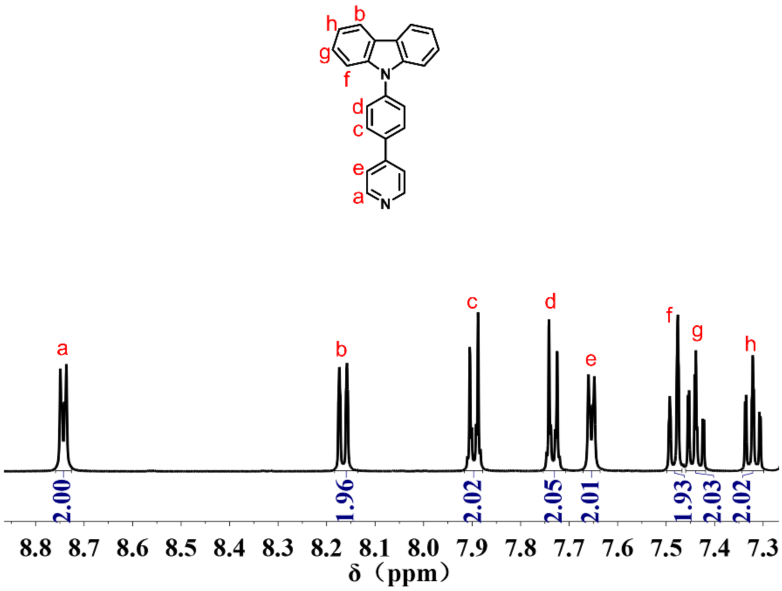

Figure S18. ^{1}H NMR spectrum of 9-(4-(pyridin-4-yl) phenyl)-9H-carbazole (**L$_1$**) in $CDCl_3$.

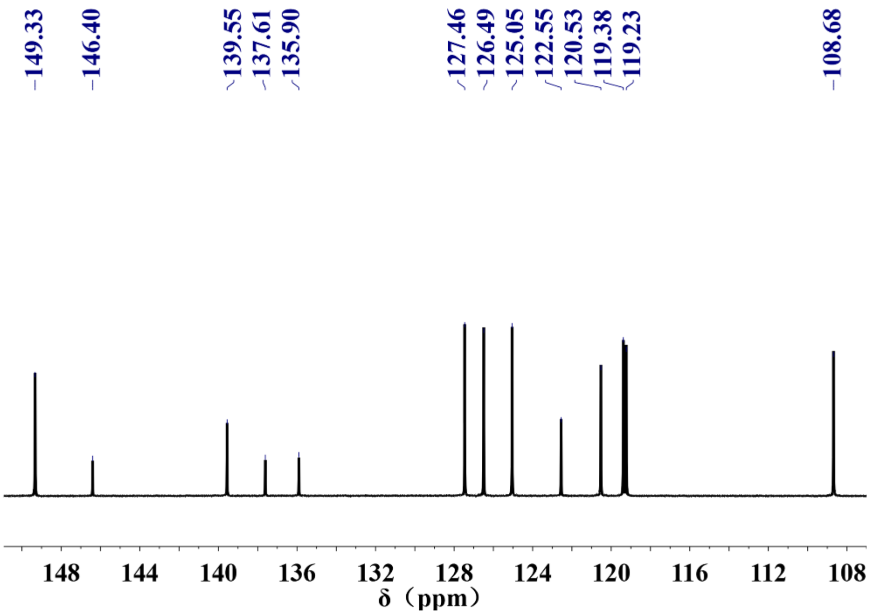

Figure S19. ^{13}C NMR spectrum of $\mathbf{L_1}$ in $CDCl_3$.

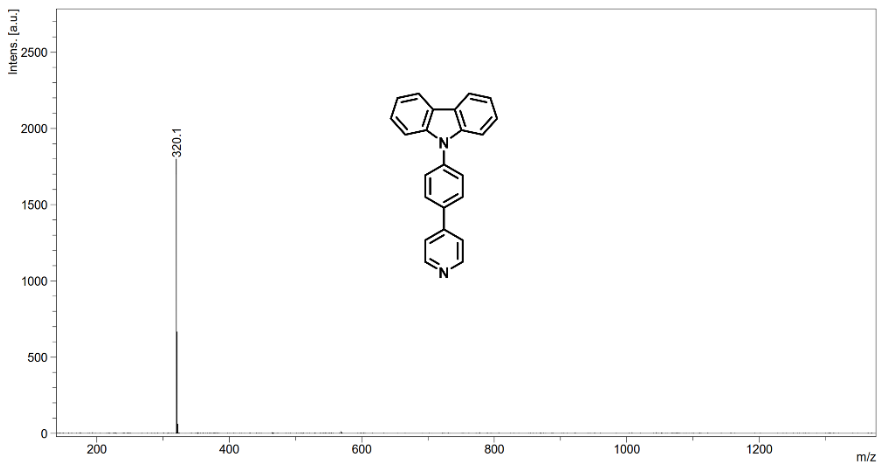

Figure S20. MALDI-TOF mass spectrum of $\mathbf{L_1}$ in CH_2Cl_2.

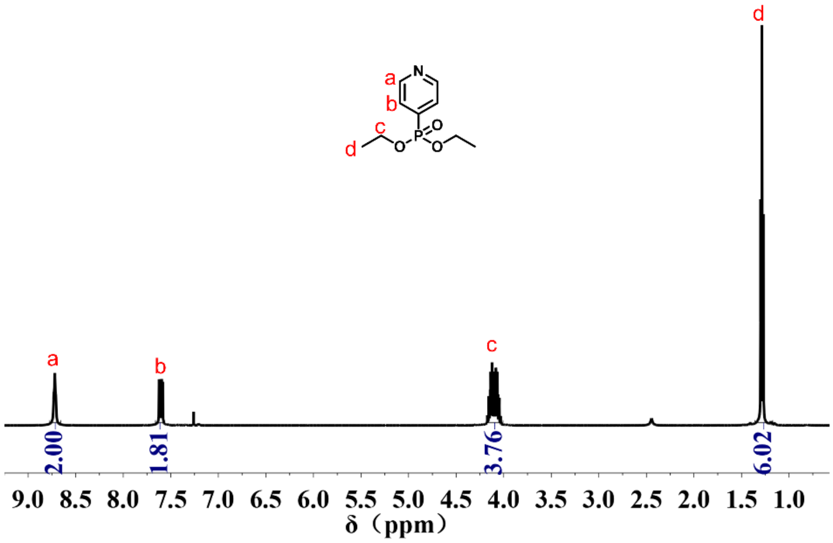

Figure S21. ^{1}H NMR spectrum of diethyl pyridin-4-ylphosphonate (**$L_{3\text{-}1}$**) in $CDCl_3$.

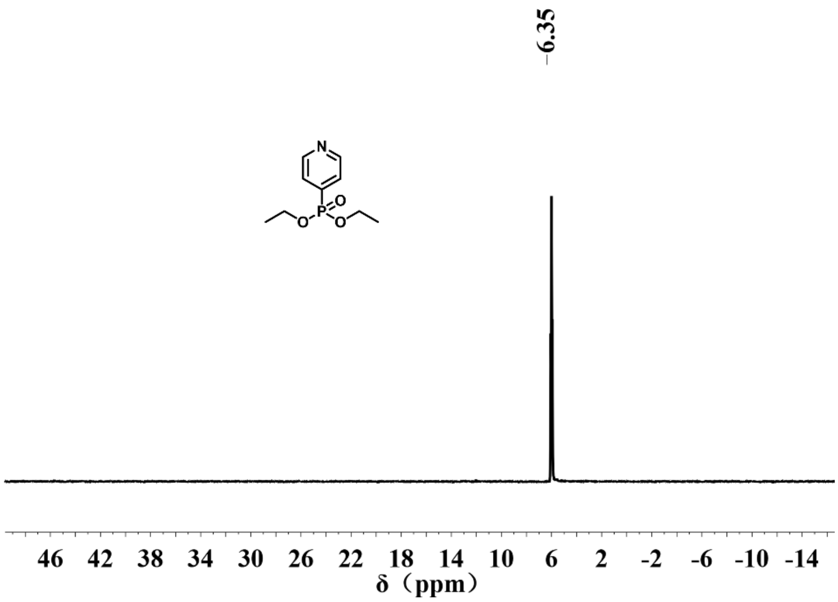

Figure S22. ^{31}P NMR spectrum of **$L_{3\text{-}1}$** in $CDCl_3$.

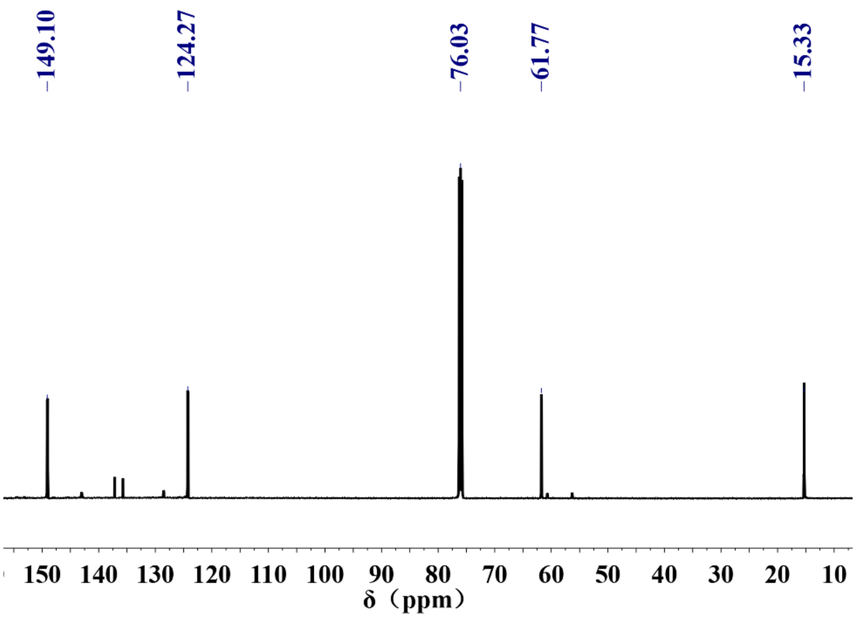

Figure S23. ^{13}C NMR spectrum of $\mathbf{L_{3\text{-}1}}$ in $CDCl_3$.

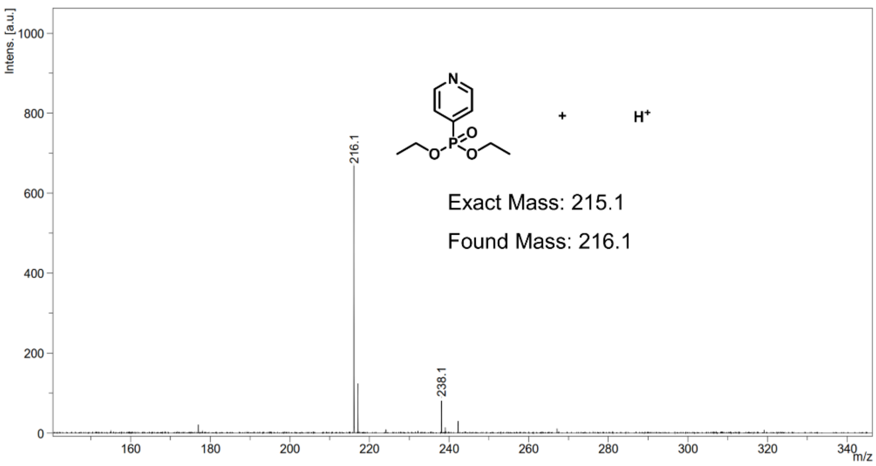

Figure S24. MALDI-TOF mass spectrum of $\mathbf{L_{3\text{-}1}}$ in CH_2Cl_2.

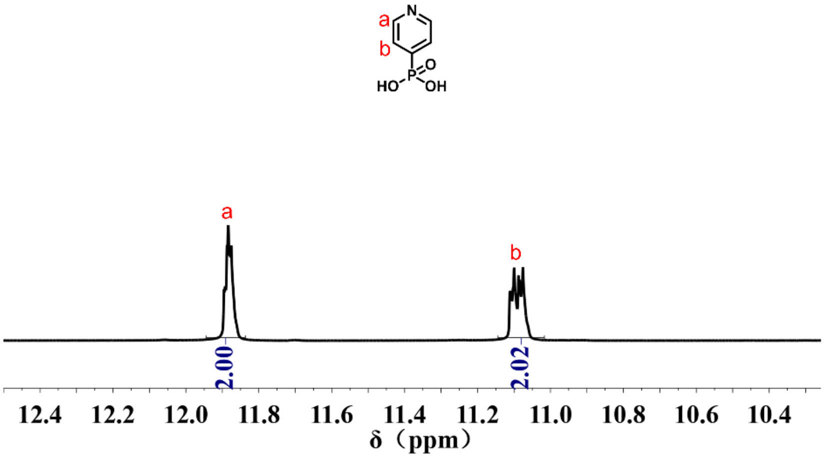

Figure S25. ^{1}H NMR spectrum of pyridyl-4-phosphonic acid (**L_3**) in $CDCl_3$.

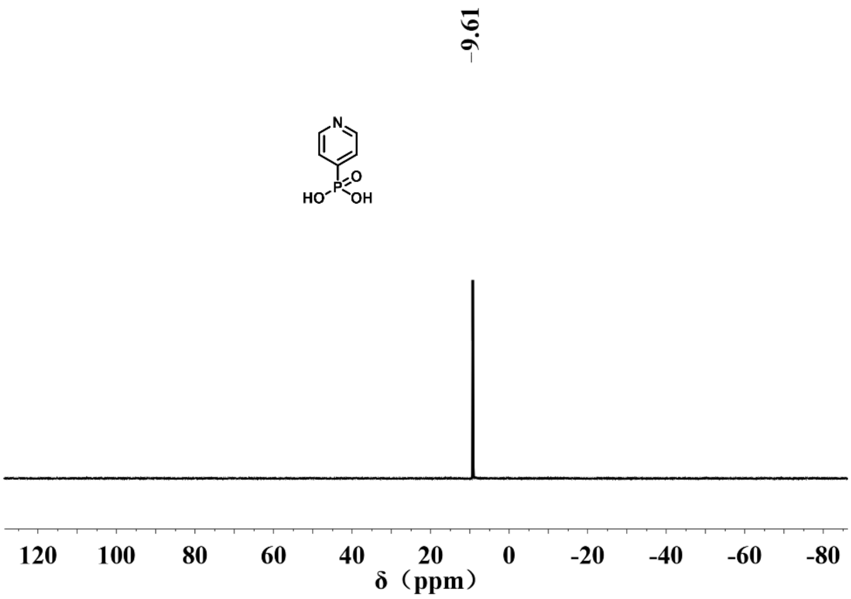

Figure S26. ^{31}P NMR spectrum of **L_3** in $CDCl_3$.

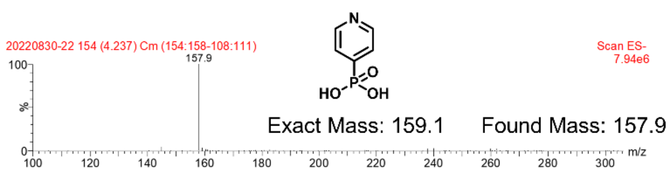

Figure S27. Electrospray ionization (ESI) mass spectrum of **L_3** in CH_3OH.

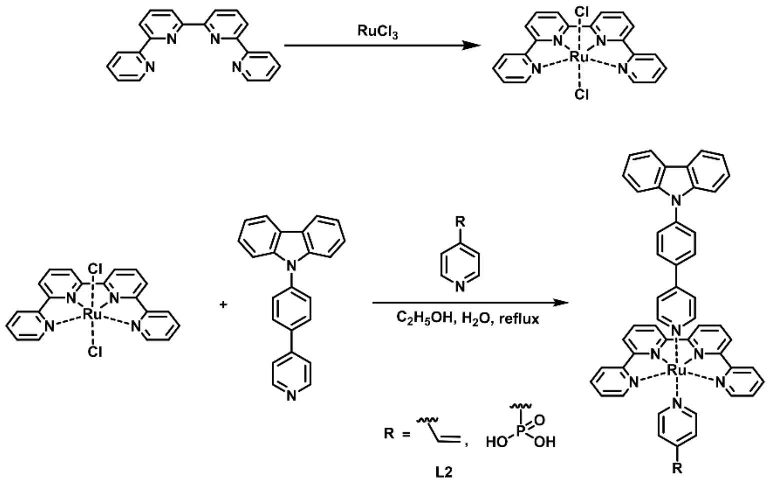

Figure S28. Synthesis routes of the Ru^{II}(qpy)L$_1$L$_2$ and Ru^{II}(qpy)L$_1$L$_3$.

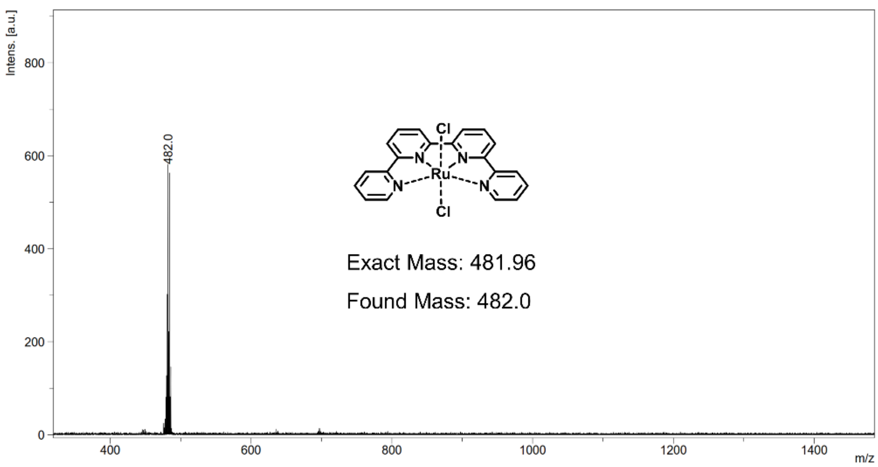

Figure S29. MALDI-TOF mass spectrum of Ru^{II}(qpy)Cl$_2$ in CH_2Cl_2.

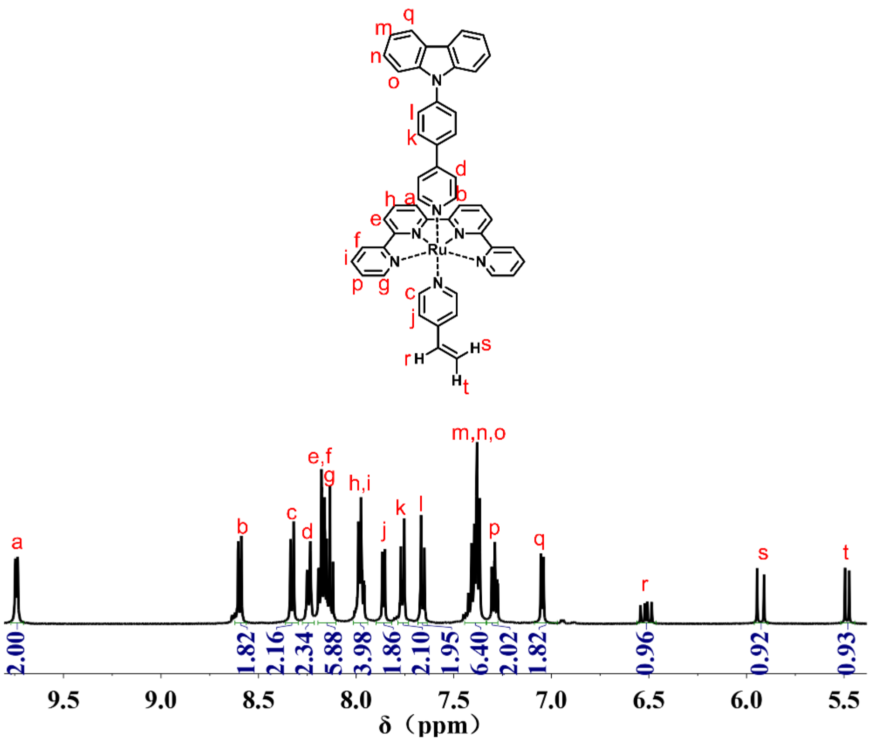

Figure S30. ^{1}H NMR spectrum of Ru$^{\mathbf{II}}$(qpy)L_1L_2 in CD_3CN.

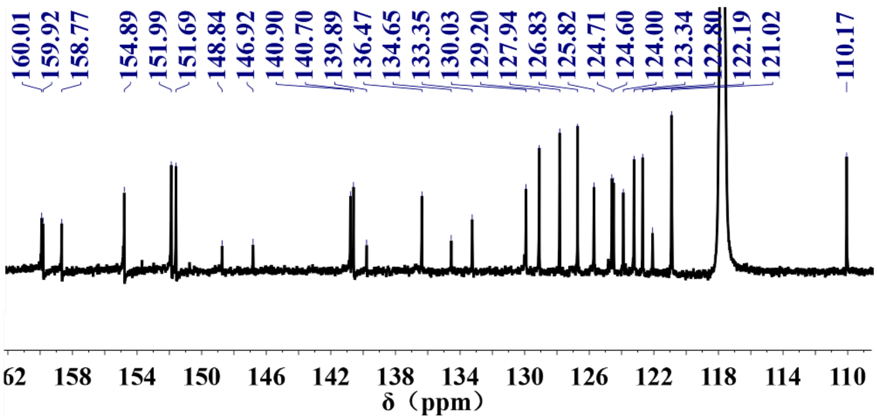

Figure S31. ^{13}C NMR spectrum of Ru$^{\mathbf{II}}$(qpy)L_1L_2 in CD_3CN.

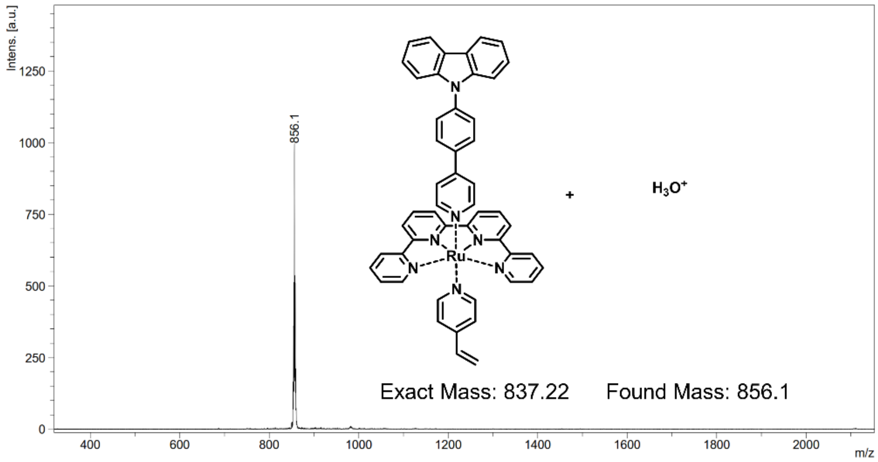

Figure S32. MALDI-TOF mass spectrum of $Ru^{II}(qpy)L_1L_2$ in CH_3CN.

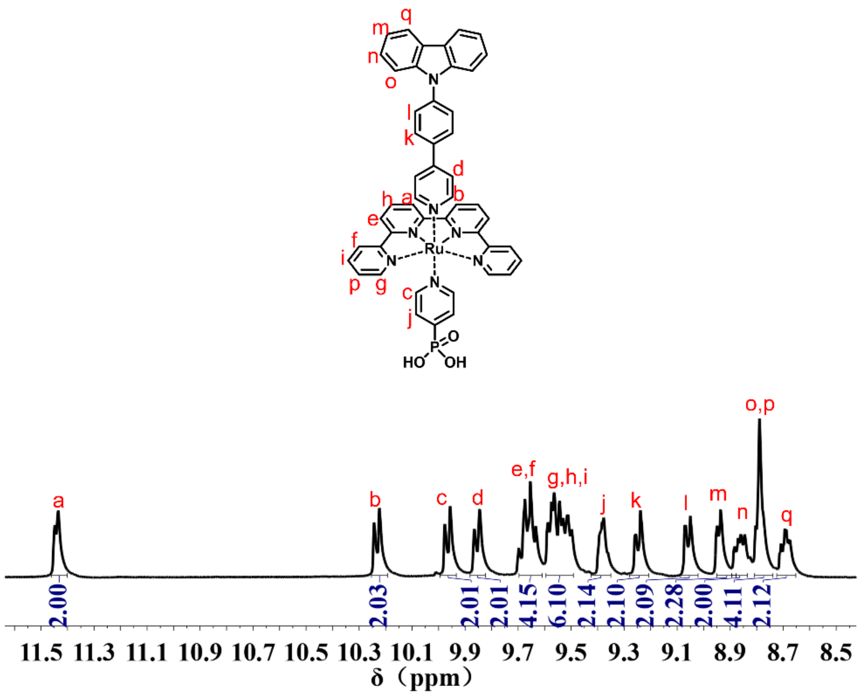

Figure S33. [1]H NMR spectrum of $Ru^{II}(qpy)L_1L_3$ in CD_3OD.

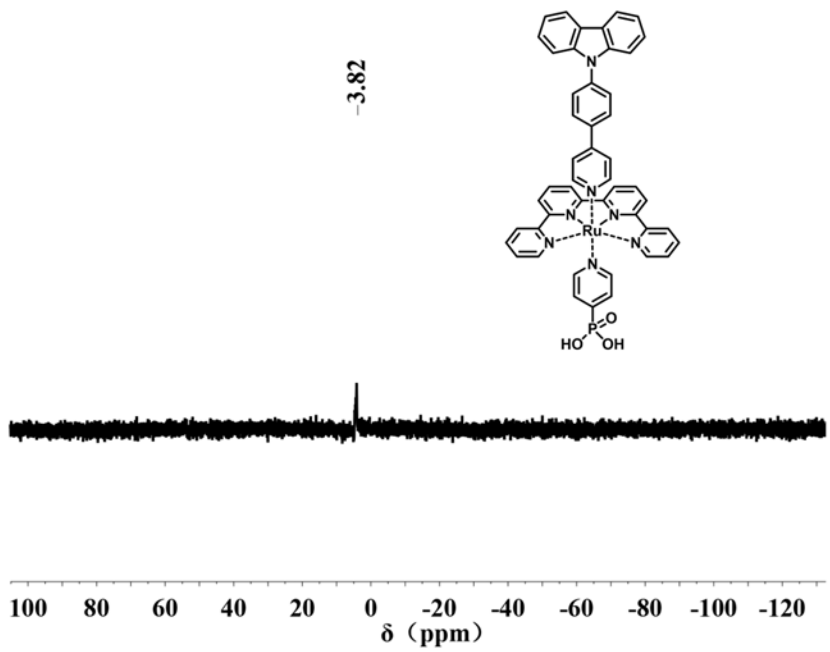

Figure S34. ^{31}P NMR spectrum of $Ru^{II}(qpy)L_1L_3$ in CD_3OD.

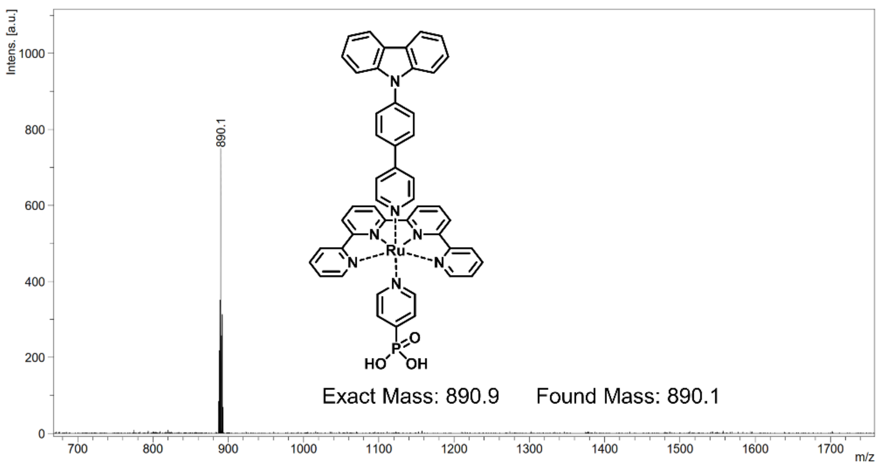

Figure S35. MALDI-TOF mass spectrum of $Ru^{II}(qpy)L_1L_3$ in CH_3OH.

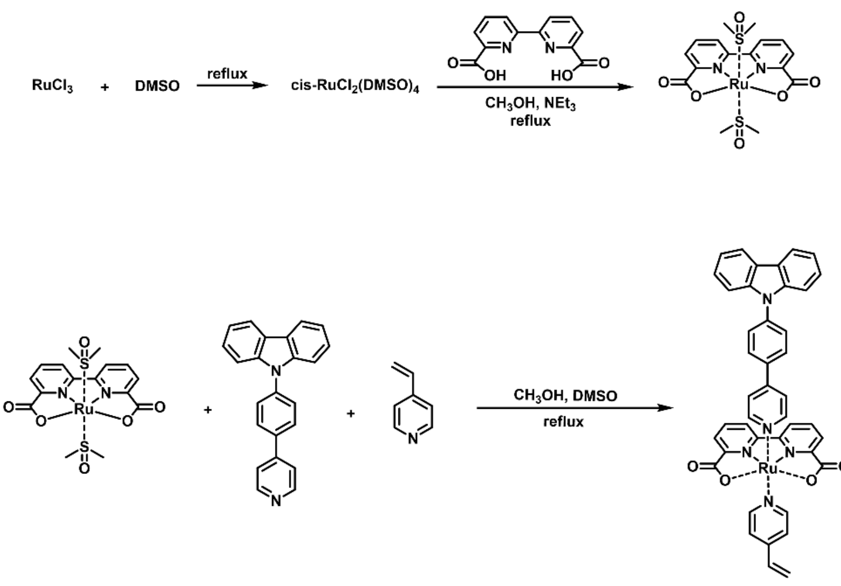

Figure S36. Synthesis routes of the $Ru^{II}(bda)L_1L_2$.

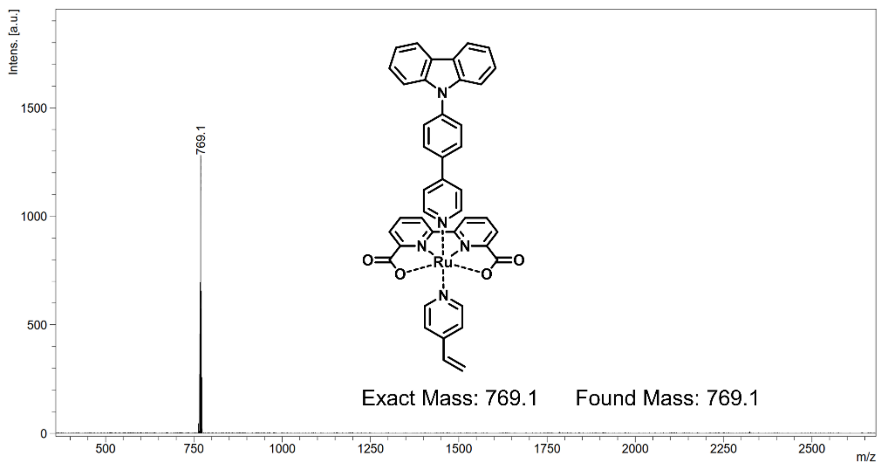

Figure S37. MALDI-TOF mass spectrum of $Ru^{II}(bda)L_1L_2$ in CH_2Cl_2.

2. Supplemental Synthesis

Commercially available solvents and reagents were used without further purification unless otherwise mentioned.

Synthesis of 2,2':6',2'':6'',2'''-quaterpyridine (**qpy**):

Qpy was synthesized using the palladium catalyzed reductive homocoupling reactions.[6] Adding 6-bromo-2,2'-bipyridine (235 mg,1.0 mM), $Pd(dppf)_2Cl_2{\cdot}CH_2Cl_2$ (81.6 mg, 0.1 mM), CsF (1.14g, 7.5 mM) and DMSO (10.0 mL) to a round bottom flask with a magnetic stir bar. The mixture was stirred at 120°C for 24 hours under argon atmosphere. The reaction was cooled to room temperature, then extracted three times with CH_2Cl_2 and H_2O. Organic layer was dried with Na_2SO_4, filtered, and concentrated. The crude product was purified by silica gel column chromatography (eluting with 60:30:1 petroleum ether/CH_2Cl_2/NH_4OH) to yield qpy as a white powder (64%). ^1H NMR (500 MHz, $CDCl_3$-d) δ 8.73 (ddd, J = 4.8, 1.8, 0.9 Hz, 2H), 8.68 (ddd, J = 7.8, 6.8, 1.1 Hz, 4H), 8.50 (dd, J = 7.7, 1.2 Hz, 2H), 8.01 (t, J = 7.8 Hz, 2H), 7.90 (td, J = 7.7, 1.8 Hz, 2H), 7.36 (ddd, J = 7.3, 4.8, 1.3 Hz, 2H). ^{13}C NMR (500 MHz, $CDCl_3$-d) δ 155.20, 154.37, 154.27, 148.08, 136.78, 135.86, 122.73, 120.17, 119.97, 75.74.

Synthesis of 9-(4-(pyridin-4-yl) phenyl)-9H-carbazole (**L_1**):

L_1 was synthesized using the classical protocol of Suzuki cross-coupling reaction.[7] Adding 4-(9-carbazolyl) benzeneboronic acid (344.6 mg, 1.2 mM), 4-bromopyridine (194.5 mg, 0.20 mM), $Pd(PPh_3)_4$ (57.8 mg, 0.050 mM), K_3PO_4 (2.6 g, 10 mM) and toluene/H_2O (20 mL/5.0 mL) to a round bottom flask with a magnetic stir bar. The mixture was refluxed with stirring overnight under argon atmosphere. The reaction was cooled to room temperature, extracted three times with CH_2Cl_2 and H_2O. Organic layer was dried with Na_2SO_4, filtered, and concentrated. The crude product was purified by silica gel column chromatography (eluting with 90:30:1 petroleum ether/CH_2Cl_2/NH_4OH) to yield L_1 as a yellow powder (90%).^1H NMR (500 MHz, $CDCl_3$-d) δ 8.76-8.73 (m, 1H), 8.17 (dt, J = 7.8, 1.0 Hz, 1H), 7.92-7.88 (m, 1H), 7.75- 7.71 (m, 1H), 7.67-7.64 (m, 1H), 7.48 (dt, J = 8.3, 1.1 Hz, 1H), 7.44 (ddd, J = 8.2, 6.9, 1.2 Hz, 1H), 7.32 (ddd, J = 8.1, 7.0, 1.2 Hz, 1H). ^{13}C NMR (500 MHz, $CDCl_3$-d) δ 149.33, 146.40, 139.55, 137.61, 135.90, 127.46, 126.49, 125.05, 122.55, 120.53, 119.38, 119.23, 108.68.

Synthesis of diethyl pyridin-4-ylphosphonate (**L_{3-1}**):

L_{3-1} was synthesized using the classical protocol of the Hirao cross-coupling reaction.[8] Adding 4'-bromopyridine (194.5 mg, 1 mM), diethyl phosphite (165.7 mg, 1.2 mM), Pd $(OAc)_2$ (4.5 mg, 0.02 mM), dppf (22.2 mg, 0.04 mM), triethylamine (0.3 mL, 2.3 mM) and CH_3CN (10 mL) to a round bottom flask with a magnetic stir bar. The mixture was refluxed by stirring for 2 days under an argon atmosphere. The reaction was cooled to room temperature, extracted three times with CH_2Cl_2 and H_2O. The organic layer was dried with Na_2SO_4, filtered, and concentrated. The crude product was purified by silica gel column chromatography (eluting with 5:1 CH_2Cl_2/NH_4OH) to yield L_{3-1} as a yellow oil (73% yield). ^1H NMR (500 MHz, $CDCl_3$-d) δ 8.84-8.73 (m, 1H), 7.67 (ddd, J = 13.4, 4.3, 1.6 Hz, 1H), 4.25-4.08 (m, 2H), 1.35 (t, J = 7.1 Hz, 3H). ^{13}C NMR (500 MHz, $CDCl_3$-d) δ 149.10, 124.27, 76.03, 61.77, 15.33. ^{31}P NMR (500 MHz, CH_3OH-d4) δ 6.06, 6.00, 5.94, 5.92.

Synthesis of pyridyl-4-phosphonic acid (**L_3**):

L_3 was synthesized by alcoholysis of L_{3-1}.[9] L_{3-1} (215 mg, 1 mM) was added to a round bottom flask with a magnetic stir bar and trimethylbromosilane (306 mg, 2 mM) was introduced via a syringe under an argon atmosphere. This mixture was refluxed by stirring for 48 hours. After cooling down, 1.0 mL methanol was injected into the mixture via a syringe and stirred for another 1 hour to complete the alcoholysis. The reaction solution was poured into a beaker containing 100 mL of ether, stirred and allowed to stand, and the supernatant was poured. Continue to add 100mL of ether to the beaker, let it stand overnight in the fume cupboard, the yellow oil became a white solid, and vacuum dried to obtain the product (100% yield). ^{1}H NMR (500 MHz, CH_3OH-d4) δ 11.88 (q, J = 6.2, 5.5 Hz, 1H), 11.09 (dd, J = 12.1, 5.2 Hz, 1H), 6.68 – 6.60 (m, 1H). ^{31}P NMR (500 MHz, CH_3OH-d4) δ 6.06, 6.00, 5.94, 5.92.

Synthesis of $Ru^{\mathbf{II}}(qpy)Cl_2$:

$Ru^{\mathbf{II}}(qpy)Cl_2$ was synthesized using a one-step coordination protocol.[10] Adding $RuCl_3·3H_2O$ (120 mg, 0.6 mM), qpy (150 mg, 0.5 mM) and ethanol (15 mL) to a round bottom flask with a magnetic stir bar was added. The mixture was refluxed under argon for 12 hours. After cooling to room temperature, the resulting precipitation was filtered, washed with H_2O and ether respectively, and vacuum dried to obtain the dark green powder (98% yield).

Synthesis of $Ru^{\mathbf{II}}(qpy)L_1L_2$:

$Ru^{\mathbf{II}}(qpy)L_1L_2$ was synthesized using a one-pot coordination protocol.[11] $Ru^{\mathbf{II}}(qpy)Cl_2$ (60 mg, 0.12 mM), L_1 (159 mg, 0.48 mM), CF_3SO_3Ag (63.7 mg, 0.24 mM), and ethanol/H_2O (35 mL/5 mL) were added to a round bottom flask with a magnetic stir bar under an argon atmosphere, L_2 (159 mg, 0.48 mM) was added at last via a syringe. The mixture was stirred at 100°C for 48 hours. The reaction was cooled to room temperature and concentrated. The crude product was purified by neutral alumina chromatography (eluting with 2:1 CH_3CN/toluene). The exchange of counterion was completed by adding saturated NH_4PF_6 aqueous solution to the resulting pure product, the precipitation was filtered, washed with H_2O and ether, then dried to yield $Ru^{\mathbf{II}}(qpy)L_1L_2$ as dark red powder (20%). ^{1}H NMR (500 MHz, CD_3CN-d3) δ 9.74 (ddd, J = 5.4, 1.6, 0.8 Hz, 2H), 8.62-8.56 (m, 2H), 8.33 (dd, J = 8.1, 0.9 Hz, 2H), 8.28-8.21 (m, 2H), 8.20-8.10 (m, 6H), 8.01-7.94 (m, 4H), 7.90-7.82 (m, 2H), 7.79-7.73 (m, 2H), 7.68-7.64 (m, 2H), 7.44-7.33 (m, 6H), 7.33-7.27 (m, 2H), 7.09-6.97 (m, 2H), 6.51 (dd, J = 17.6, 10.9 Hz, 1H), 5.93 (d, J = 17.6 Hz, 1H), 5.48 (d, J = 10.9 Hz, 1H).^{13}C NMR (500 MHz, CD_3CN-d3) δ 160.01, 159.92, 158.77, 154.89, 151.99, 151.69, 148.84, 146.92, 140.90, 140.70, 139.89, 136.47, 134.65, 133.35, 130.03, 129.20, 127.94, 126.83, 125.82, 124.71, 124.60, 124.00, 123.34, 122.80, 122.19, 121.02, 110.17.

Synthesis of $Ru^{\mathbf{II}}(qpy)L_1L_3$:

$Ru^{\mathbf{II}}(qpy)L_1L_3$ was synthesized using a one-pot coordination protocol. $Ru^{\mathbf{II}}(qpy)Cl_2$ (60 mg, 0.12 mM), L_1 (159 mg, 0.48 mM), L_3 (76.3 mg, 0.48 mM), CF_3SO_3Ag (63.7 mg, 0.24 mM), and ethanol/H_2O (35 mL/5 mL) were added to a round bottom flask with a magnetic stir bar. The mixture was refluxed by stirring for 2 days under an argon atmosphere. The reaction was cooled to room temperature and concentrated. The crude product was purified by silica gel column chromatography (eluting with 10:5:1 $CH_3CN/CH_3OH/NH_4OH$). The exchange of counterion was completed by adding saturated NH_4PF_6 aqueous solution to the resulting pure product, the precipitation was filtered, washed with H_2O, ether, and dried to yield

Ru^{II}(qpy)L_1L_3 as dark red powder (30%). ^{1}H NMR (400 MHz, CH_3OH-d4) δ 11.44 (d, J = 5.6 Hz, 1H), 10.25-10.19 (m, 1H), 9.99-9.93 (m, 1H), 9.85 (d, J = 8.1 Hz, 1H), 9.70-9.61 (m, 2H), 9.60-9.49 (m, 3H), 9.38 (dt, J = 8.9, 4.1 Hz, 1H), 9.28-9.21 (m, 1H), 9.09-9.02 (m, 1H), 8.95-8.88 (m, 1H), 8.89-8.84 (m, 1H), 8.81-8.74 (m, 2H), 8.70 (dt, J = 10.1, 4.0 Hz, 1H).^{31}P NMR (500 MHz, CH_3OH) δ 3.82.

Synthesis of Cis-$Ru^{II}Cl_2(DMSO)_4$ and Ru^{II}(bda)$(DMSO)_2$:

Cis-$Ru^{II}Cl_2(DMSO)_4$ and Ru^{II}(bda)$(DMSO)_2$ were synthesized according to previous literature.[6] Firstly, $RuCl_3{\cdot}3H_2O$ (2.07 g, 10 mM) and DMSO (10 mL) were added to a round bottom flask with a magnetic stir bar under an argon atmosphere. This mixture was refluxed by stirring for 5 minutes. The reaction was cooled to room temperature and concentrated. After adding 20 mL of acetone, the precipitation was generated, which was filtered, washed with H_2O, ether and dried to yield as yellow powder Cis-$Ru^{II}Cl_2(DMSO)_4$. Secondly, 2,2'-bipyridine-6,6'-dicarboxylic acid (100 mg, 0.41 mM), Cis-$Ru^{II}Cl_2(DMSO)_4$ (200 mg, 0.41 mM), triethylamine (0.3 mL) and CH_3OH (20 mL) were added to a round bottom flask with a magnetic stir bar. The mixture was refluxed by stirring for 4 hours under an argon atmosphere. After cooling to room temperature, the resulting sediment was filtered, washed with H_2O and ether respectively, and vacuum dried to obtain the yellow powder Ru^{II}(bda)$(DMSO)_2$ (80% yield).

Synthesis of Ru^{II}(bda)L_1L_2:

Ru^{II}(bda)L_1L_2 was synthesized using a one-pot coordination protocol. Ru^{II}(bda)$(DMSO)_2$ (50 mg, 0.1 mM), L_1 (35.2 mg, 0.11 mM) and CH_3OH/DMSO (10 mL/0.1 mL) were added to a round bottom flask with a magnetic stir bar under an argon atmosphere, L_2 (11 mg, 0.1 mM) was added at last via a syringe. The mixture was refluxed by stirring for 4 hours. The reaction was cooled to room temperature and concentrated. The crude product was purified by silica gel column chromatography (eluting with 15:1 CH_2Cl_2/CH_3OH) to yield Ru^{II}(bda)L_1L_2 as a red powder (30% yield).

3. Supplemental Methods

The preparation of self-assembled monolayers (SAMs)

The indium tin oxide (ITO) substrates were immersed in 0.1 mM phosphonates complex (Ru(II)-qpyL_1L_3) CH_3OH solution for 24h at room temperature, washed with CH_3OH and CH_2Cl_2, and then sonicated in CH_3OH for 5 min.

General Characterizations

^{1}H, ^{13}C, and ^{31}P nuclear magnetic resonance (NMR) spectra of organic molecules and complexes were measured with a Bruker AV-500 spectrometer. Matrix-assisted laser desorption ionization-time-of-flight (MALDI-TOF) and electrospray ionization (ESI) mass spectra of organic molecules and complexes were obtained using a Bruker. Daltonics Autoflex III TOF. UV-vis absorption spectra were recorded on a

JASCO V-770 spectrophotometer. Atomic force microscopy (AFM) images were collected from a Bruker Dimension Icon. Infrared reflection absorption spectrometry (IR-RAS) was recorded using a Bruker ALPHA II. Bruker ALPHA II. Scanning electron microscopy (SEM) measurements were carried out with an S-4800 high-resolution field emission scanning electron microscope.

Electrosynthesis

The electrosynthesis was carried out in a three-electrode setup (Ag/Ag+ as the reference electrode, platinum foil as the counter electrode, and ITO as the working electrode) with a CHI660E electrochemical analyzer system. The reaction cell was 5 mL of CH_3CN or CH_2Cl_2 solution containing 0.5 mM monomer and 0.1 M Bu_4NClO_4. Electrosynthesis was initiated from SAMs on ITO. By switching alternative redox reactions using cyclic voltammetry (CV) mode, including the oxidative reaction of carbazoles and the reductive reaction of vinyl in their solutions, the monolayers grew in one-by-one addition of target monomers. The potential sweeping ranges, scan rates, and solvent species were as follows: −0.4–1.1 V, 35 mV/s in CH_3CN for R_1 oxidative self-coupling; −0.4–1.1 V, 35 mV/s in CH_2Cl_2 for R_2 oxidative self-coupling; −1.8–0 V, 40 mV/s in CH_3CN for R_1 reductive self-coupling. Each reaction takes 1–2 min. Before the reduction reaction, the working electrode surface was purged with argon for 15 min to remove oxygen. The working electrode must be rinsed with CH_3CN and dried with argon to eliminate unreacted monomers and by-products. The oxidation potential may increase (c.a. 0.1 V) for long molecules to ensure the full coverage reaction as much as possible because of the resistance increase. Usually, CH_3CN was chosen as a solvent for electrochemical reactions. However, R_2 had good solubility only in CH_2Cl_2. Thus, only an oxidative reaction in CH_2Cl_2 was available because CH_2Cl_2 is unstable for reductive reactions with a range of negative potentials.

Electrocatalytic water oxidation

Electrocatalytic water oxidation was conducted in a three-electrode setup (Ag/AgCl as the reference electrode, platinum wire as the counter electrode, and monolayers as the working electrode) with linear sweep voltammetry (LSV) mode. LSV measurement was carried out on monolayer/ITO in a 0.1 M $HClO_4$ aqueous solution at pH = 1.0 with a scan rate of 20 mV/s. The potentials were converted to the reversible hydrogen electrode (RHE) scale via calibration ($E_{\mathrm{RHE}} = E_{\mathrm{Ag/AgCl}} + 0.059$ pH + 0.197). Overpotential (η) was calculated by the difference between the actual reaction potential (E_{onset}): $\eta = E_{\mathrm{onset}} - 1.23 + 0.059$ pH).[12]

4. Supplemental References

1 C. W. Chan, T. F. Lai and C. M. Che, *J. Chem. Soc.-Dalton Trans*, 1994, 895-899.

2 Y. Pineda-Galvan, A. K. Ravari, S. Shmakov, L. Lifshits, N. Kaveevivitchai,

R. Thummel and Y. Pushkar, *J. Catal*, 2019, **375**, 1-7.
3 L. P. Tong, R. F. Zong, R. W. Zhou, N. Kaveevivitchai, G. Zhang and R. P. Thummel, *Faraday Discuss*, 2015, **185**, 87-104.
4 J. T. Muckerman, M. Kowalczyk, Y. M. Badiei, D. E. Polyansky, J. J. Concepcion, R. F. Zong, R. P. Thummel and E. Fujita, *Inorg. Chem*, 2014, **53**, 6904-6913.
5 H. W. Tseng, R. Zong, J. T. Muckerman and R. Thummel, *Inorg. Chem*, 2008, **47**, 11763-11773.
6 C. Z. Qi, X. D. Sun, C. Y. Lu, J. Z. Yang, Y. J. Du, H. J. Wu and X. M. Zhang, *J. Organomet. Chem*, 2009, **694**, 2912-2916.
7 K. Leduskrasts, A. Kinens and E. Suna, *Chem. Commun*, 2019, **55**, 12663-12666.
8 P. Finkbeiner, J. P. Hehn and C. Gnamm, *J. Med. Chem*, 2020, **63**, 7081-7107.
9 J. Zhang, J. X. Wang, C. Wei, Y. F. Wang, G. Y. Xie, Y. F. Li and M. Li, *Nat. Commun*, 2020, **11**, 8.
10 Y. Y. Liu, S. M. Ng, S. M. Yiu, W. W. Y. Lam, X. G. Wei, K. C. Lau and T. C. Lau, *Angew. Chem. Int. Ed*, 2014, **53**, 14468-14471.
11 J. Zhang, J. Du, J. X. Wang, Y. F. Wang, C. Wei and M. Li, *Angew. Chem. Int. Ed*, 2018, **57**, 16698-16702.
12 Q. Q. Shi, Z. B. Zhang and S. Y. Liu, *Angew. Chem. Int. Ed*, 2024, **63**, 18.